Laser-induced damage of PMMA on borosilicate glass

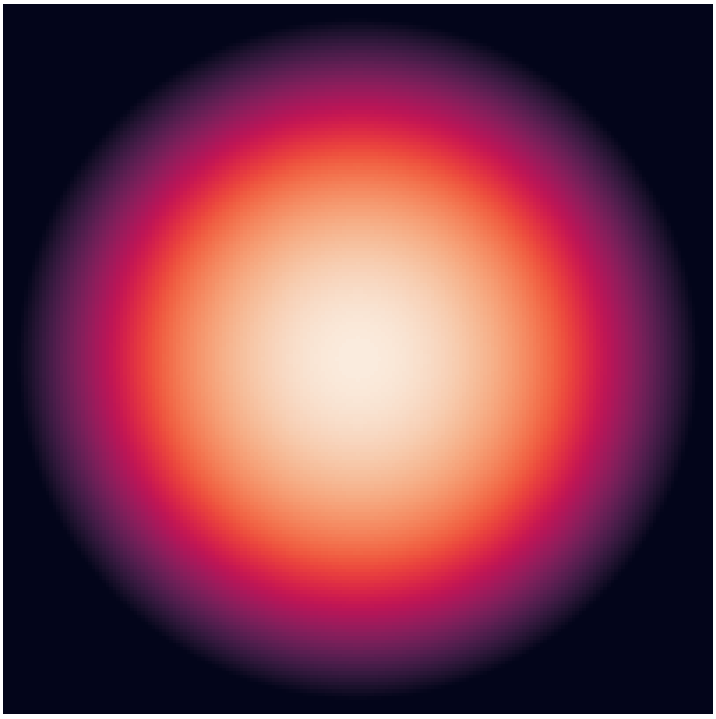

Tom Hommes
Supervisors: Dr. D. van Oosten, Dr. E.M. Hutter
Daily Supervisor: M.C.W. Vreugdenhil

June 2022

Abstract

In this thesis we investigate the the light induced damage threshold (LIDT) of PMMA on borosilicate glass at different pulse lengths. PMMA is a electron beam resist widely used in the semiconductor industry (15). This makes PMMA an interesting compound to examine. In this thesis we expose both PMMA on borosilicate glass and bare borosilicate glass (as a reference measurement) to light at different pulse lengths and fluences. We examine these illuminated sites by optical profilometric microscopy depth maps and optical transmission images. We find separate LIDTs for PMMA on borosilicate glass using a Liu analysis and using anther fit based on crater radius. For borosilicate glass, we find a LIDT by selecting site of first damage from profilometry and transmission images. We also find an LIDT for borosilicate glass from optical images taken of self-reflectivity of the sample during the pulse. We also determine a stochastic behavior in the ablation for both PMMA on borosilicate glass and borosilicate glass. Through an experiment exposing PMMA on borosilicate glass to light with different pulse lengths and fluences, for 32 sites at the time, we were able to find a damage probability for the different pulse lengths and fluences.

Contents

1 Introduction

The semiconductor industry is interested the production of increasingly smaller chips. To do so, high intensity light sources are needed in the meteorological process. Pulsed laser are ideal for this process, except for the possible ligth-induced damage (LID) to the material they cause. Because of this, it is important to understand LID for materials used in the semiconductor industry. PMMA is widely used in the semiconductor industry as a positive electron beam resist on wafers. An electron beam resist is a compound which undergoes a chemical reaction when exposed to electron beams. This chemical reaction makes the compound more or less soluble. In the case of a positive electron beam resist, the compound becomes soluble upon exposure. A negative resist becomes less soluble after exposure to an electron beam. Because of this property, PMMA is commonly used as positive resist in lithography of microchips. PMMA can also be used as a negative resist when treated differently (15). To map positions of the wafer before the lithography, lasers are being used ((ASML)). LID is dependent on several parameter. However, it is known that for a lot of polymers, like PMMA, the light induced damage thresholds (LIDT) also reduces with lowering of the pulse length (7). For this reason, we investigate light induced damage in a thin layer of PMMA, on a borosilicate glass substrate. We do this in order to get a better understanding of the processes going on at high fluences in the femtosecond, picosecond pulse length regime.

We examine both PMMA and its bare substrate borosilicate glass for illuminations for different fluences at different pulse lengths. For PMMA on borosilicate glass, we analyse any damage which occurs due to illumination. We do this by looking at depth maps from an optical profilometer and in situ aftermath images. We determine the single-shot LIDTs as a function of pulse length for both PMMA on borosilicate glass and for bare borosilicate glass.

We find that ablation of PMMA becomes a stochastic process at pulse lengths from 3 ps and higher at certain fluences. We examine this stochastic behavior by determining the damage probability at a regime of different pulse lengths and fluences where this stochastic process takes place.

2 Theory

In this thesis we aim to get a better understanding of light induced damage to PMMA for different pulse lengths. In this chapter we explain the relevant physical and chemical properties of PMMA and its substrate, borosilicate glass. Then, we explain our definition of light-induced damage (LID). After that, we explain a common method of finding the light-induced damage threshold (LIDT) of a material. We conclude this chapter by explaining the mechanisms behind the LID.

2.1 Properties of PMMA and borosilicate glass

Polymethyl methacrylate (PMMA) is polymer, which is transparent for VIS- and IR-light (4). According to (26), the single-shot LIDT has previously been determined to be 2.05 $\pm$ 0.23 J cm^{-2}. This value has been determined for a pulse length of 343 fs with a wavelength of 1030 nm.
There is a relatively large difference in bandgaps for PMMA in literature. The bandgap of PMMA on SiO_2 is about 4.0 eV according to (1) and for bare PMMA it is said to be between 4.2 $\pm$ 0.1 using different methods to determine this value. In (26) the bandgap of PMMA is said to be 5.21 eV.
Its melting point increases with degree of polymerization (21). Starting from 220 °C, PMMA can start to to decompose if it contains unsaturated terminal C-C bonds. If the terminal bonds are saturated, the decomposition temperature is higher. In Fig. 1, the reaction for thermal decomposition of PMMA is displayed (2).

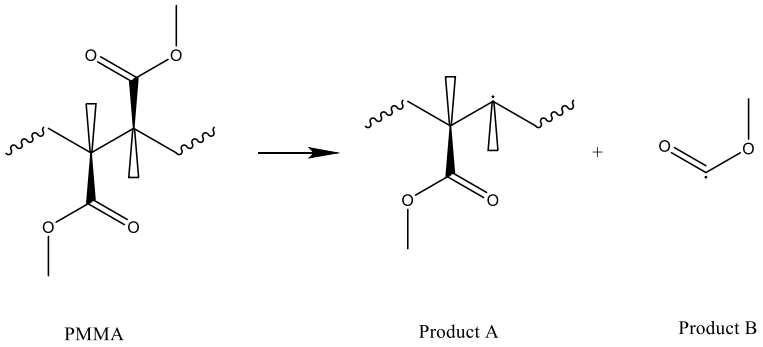

Figure 1: Decomposition reaction of PMMA to 2 radical products.

Product B can react further along 2 reaction paths. Along one path, it reacts to CO and methane in presence of H. Along the other path, it reacts to CO_2 and a methanol in presence of H. In Fig. 2, we show how product A undergoes further decomposition ((25)).

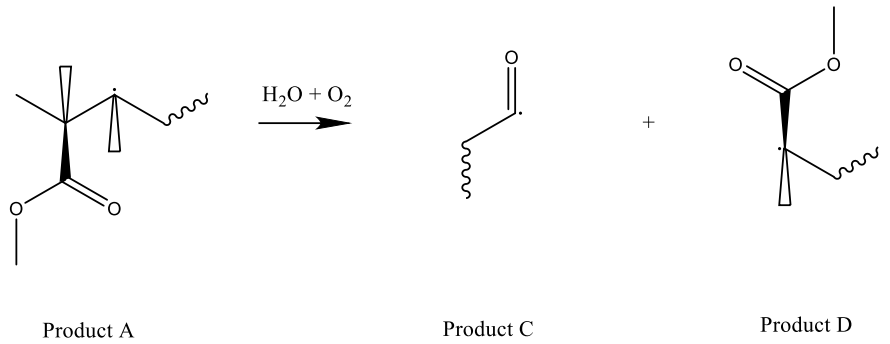

Figure 2: Further decomposition in presence of water and oxygen reaction product B to more radical products.

The newly formed radicals can radicalize other PMMA molecules or radicalize other parts in it's own molecule. It is reasonable to assume that the products C and D have a lower melting point than the original PMMA because these products are smaller in size than the original PMMA. Fig. 1 and 2 show both reactions which produce radicals. Based on findings in (9), it is safe to assume both reactions to be exothermally driven.
As mentioned earlier, the substrate of the sample that we use in our experiments is borosilicate glass. This is glass consisting of SiO_2 and B_2O_3, but usually contains other molecules as well. When referring to glass in this thesis, we will mean borosilicate glass. The bandgap of borosilicate glass is about 4.1 eV (5) and according to (11) it has a bandgap of about 4 eV. According to (22), borosilicate glass has a melting point of about 1100 K, while (6) states the melting point is 900-1000 °C (1173-1273 K). According to ((13)), the LIDT of borosilicate glass for single-shot pulses is about 2.98 J cm^{-2}. This value was determined for a pulse length of 500 fs at a wavelength of 1030 nm.
The ratio of SiO_2 to B_2O_3 for borosilicate glass is not always consistent. Considering this and the presence of other molecules, differing per sample, the above properties might be different from the borosilicate glass we use. This also explains the large differences in property values we find in literature.

2.2 Our definition of damage

In this thesis, we take a look at the LIDT of PMMA and borosilicate glass. For the semiconductor industry, the most interesting form of damage is when a compound permanently lost its function. Damage could be due to physical damage (melting, spallation, cracking), due to chemical damage (change of compound) or a combination of both. In this thesis, we chose per experiment a different way to define damage. For PMMA, we chose damage to be morphological change in the material, from which we determine two different LIDTs. For two types of damage for borosilicate glass, we each determine a LIDT. One LIDT is also determined by morphological change. The second LIDT is based on optical contrast in transmission.
The square of the radius of the crater (r) increases with logarithm of the fluence (F) (12). For damage based on morphological change, the LIDT is then defined by the intersection of this curve with the x-axis.

2.3 Light induced damage mechanisms

In this section we explain light induced damage (LID) by light with a photon energy which is lower than the bandgap energy of the exposed compound.
Upon illumination, an electron is ionized by photons from an external light source from the valence band to the conduction band. This happens on the timescale of femtoseconds (16). The minimal energy required for ionization is the bandgap energy. The ionization rate $\frac{\mathrm{d}N}{\mathrm{d}t}$ is the time derivative of the conduction band electron density. If the photon energy of the external light is lower than the bandgap energy, the simultaneous

absorption of several photons is required to promote an electron from the valence band to the conduction band. This process is referred to as Multi photon ionization (MPI). This type of ionization is usually described by the theory of Keldysh (14). This theory states that $\frac{\mathrm{d}_N}{\mathrm{d}t}$ is proportional to I^m, where m is the number of photons required to bridge the bandgap energy ((8)). Peak intensity decreases with increasing pulse length. That means that we expect to find a higher conduction band electron density at shorter pulse lengths. This would then expect us to find a lower LIDT at shorter pulse lengths.

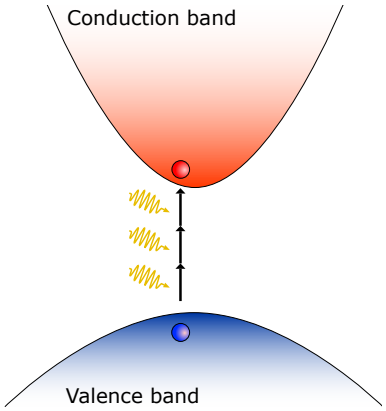

Figure 3: Multi photon ionization of electron from a parabolic valence band to parabolic conduction band (23)

Once an electron is in the conduction band, it can absorb single photons directly. This linear absorption process is also referred to as electron heating. Electron heating can occur as soon as the conduction band electron density is sufficiently high. This happens on the femtosecond timescale as well (16). Once an electron is in the conduction band, it no longer requires a photon to have a minimum energy to absorb it. This leads to a linear increase in photon absorption as a function of N.
An electron in the conduction band can do two things. It can start to ionize other electrons from the valence band to the conduction band. This is called impact ionization (17), (24).

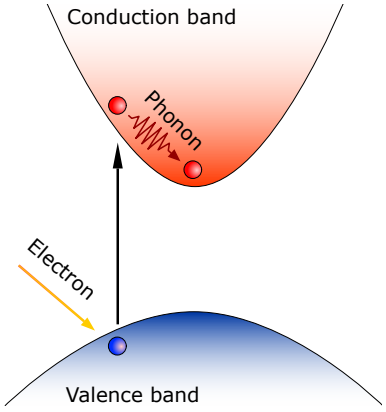

Figure 4: A visual representation of impact ionization (23)

Another option for an conduction band electron, is heating the molecular lattice via electron-phonon interaction (10). This happens on a timescale of picoseconds (16) and can result into melting of the material. Materials can also have defects. These defects can both be intrinsic or they can be insinuated by the external light source. These defects can result in trap states. Trap states are energy levels within the bandgap of the

material. A particle can fall back to the valence band in several steps via these trap states. Another option is that an electron from the valence band can be promoted to the conduction band in several steps. This type of ionization requires a lower-order absorption process than MPI does (17).

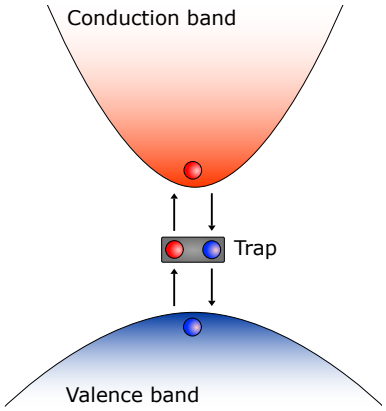

Figure 5: A visual representation of electrons and holes entering and leaving a trap state (23)

Another form of damage due to imperfections is damage due to the presence of inclusions. One scenario is that of a dust particle of some sort being present on the material. This inclusion can heat up upon exposure to light. Heat transfer of this speck can cause melting or cracking of the material underneath (18). If defects and inclusions are more or less randomly distributed and the typical distance between defects is larger than the diameter of the focus, illuminating a defect becomes probabilistic. The presence of a defect state or an inclusion within the illuminated area, can locally lower the LIDT of a material. Therefore, ablation can become a stochastic process at lower peak intensities (19). The intensity of a beam decreases as a function of pulse length. Because of this, we expect illumination to become more stochastic as a function of pulse length.

3 Experiment

The goal of the performed experiments is to find single-shot light-induced damage thresholds (LIDT) of PMMA and glass for different pulse lengths (τ) and fluences (F). We do this by illuminating a sample around τ and F of LIDTs found in literature.

3.1 Experimental Setup

In Fig. 6 we show the setup we used for illumination of a sample:

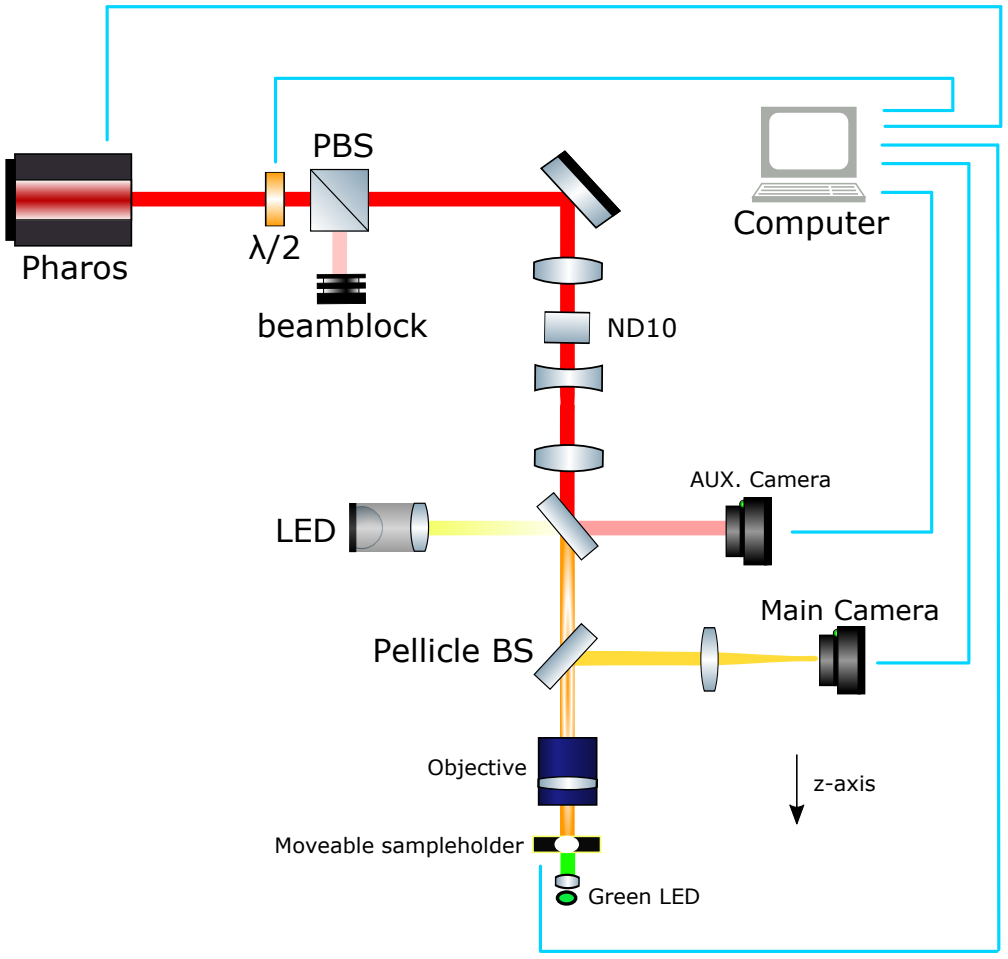

Figure 6: A schematic overview of the setup we use in our experiments

In Fig. 6 we use a *Light Conversion Pharos PH2-SP-1mJ* laser, which produces pulses at a wavelength of 1030 nm. The pulse duration of the pulses can be tuned between values between approximately 200 fs and 24 ps. The pulse length is >190 fs and the repetition rate is 1 MHz. The maximum output power of the *Light Conversion Pharos PH2-SP-1mJ* laser is 10 W.

By using a rotatable $\frac{\lambda}{2}$ waveplate, mounted on a rotation stage, followed by polarising beam splitter (PBS), we can regulate the pulse energy. We are able to regulate the beamwaist with a convex-concave-convex lenses series. Between the first convex lens and the concave lens, we use a *Thorlabs ND10* neutral density filter to attenuate the pulse energy of the beam.
We use 2 pellicle beampsplitters in the setup, both with an angle of 45° with respect to the pathway of the beam. The first pellicle beamsplitter splits a part of the beam to a CMOS camera chip, which we denote as auxiliary camera in Fig.6. We use this auxiliary camera to measure the pulse energy. This configuration allows us to measure pulse to pulse fluctuations in pulse energy. The part of the beam that is transmitted by both pellicle beam splitters, is projected on the sample by a *Nikon CFI60 100x* microscope objective. As shown in Fig. 6, we place the z-axis along the trajectory of the beam on the sample.
The sample holder can be moved along the xy-plane. The sample holder can be tilted in the xy-plane, to allow us to keep the sample in the focal plane. We can also move the microscope objective in the z-direction in order to focus the beam. Any excitation light that is reflected from the sample, is reflected by the second beamsplitter into an *Andor iXon3 885* camera. We denote this camera as the main camera. Furthermore, we use a low intensity white LED to illuminate the sample. Light produced by the LED is coupled onto the beam path using the first pellicle beamsplitter, as can be seen in Fig. 6.
By moving the sample around the xy-plane, 64 illumination sites can be created in an experiment. One field of 64 illumination sites is considered to be one run. In a typical experiment 64 runs were shot. This allows us to choose a fast parameter and a slow parameter. In an isolated run the fast parameter is the variable that is chosen to be varied between each illumination site. For each run, the fast parameter is varied in the same fashion. In a typical experiment the fast parameter is the pulse energy. The slow parameter is a variable that is varied between each run, but kept constant between shots within a run. A typically used slow parameter is pulse length.
The main camera took an image before, during and after illumination. For all images, the white LED reflection provided light for reflection. In some experiments, also a green LED illuminated the sample from behind, giving a transmission signal. The auxiliary camera took an image during an illumination (27).

4 Results

The aim of this work is to investigate light-induced damage (LID) to PMMA on borosilicate glass. We use illumination of borosilicate glass as a reference measurement. We investigate the LID by looking at damage as a function of both pulse length (τ) and fluence (F). We expect the light-induced damage threshold (LIDT) to be strongly dependent on τ. We analyse our data by looking at depth maps from an optical profilometric microscope and images taken before, during and after illumination of the sample-site. We determine a LIDT of PMMA on borosilicate glass by doing a Liu analysis on the data. We determine another LIDT of PMMA on borosilicate glass by doing a fit which keeps the beamwaist fixed in calculations. For borosilicate glass we determine the LIDT for different pulse lengths using the same fixed beamwaist fit as for PMMA on borosilicate glass. For borosilicate glass, we also determine the LIDT for different pulse lengths using self-reflectivity images of the sample during the pulse. Furthermore, we investigate the stochastic behaviour we observe at larger pulse lengths for both PMMA on borosilicate glass. For the PMMA on borosilicate glass, we determined a damage probability for different τ. From self-reflectivity images, we find a difference in damage processes for PMMA on glass and for bare borosilicate glass.

4.1 Damage analysis for PMMA on glass for different pulse lengths

Our aim is to investigate LID for PMMA on borosilicate glass for different fluences and pulse lengths. We execute our experiments by using the setup introduced in section 3. In our analysis, we use profilometry height maps and images taken during and after illumination.

4.1.1 Ablation of PMMA on glass

The sample that we investigate in our experiment is a 30 nm thick PMMA layer, spincoated onto a borosilicate glass substrate. The roughness of the sample is unknown, but the sample appears smooth in the optical profilometer. As a fast parameter, we use the pulse energy. That means that we linearly increase pulse energy from 9.20 nJ to 2.59 µJ in each run. We used the pulse length as the slow parameter. We did 4 runs for each pulse duration. In table 4.1.1 the runs with corresponding pulse lengths are shown.

Run	1-4	5-8	9-12	13-16	17-20	21-24	25-28	29-32
Pulse length	200 fs	1 ps	2 ps	3 ps	4 ps	5 ps	6 ps	7 ps

Pulse lengths longer than 7 ps did not result in distinguishable damage in profilometry data and aftermath images. Because of this, we don't include pulse lengths longer than 7 ps into the analysis.

4.1.2 Determination of the fluence

We're not interested in the LIDT of a sample of particular size, but rather in the LIDT as an intrinsic property of PMMA on borosilicate glass. Because of this we want to express the LIDT in fluence instead of pulse energy. This makes it easier to compare the determined LIDT in this work with literature.
We determine the pulse energy by integrating the camera signal from the auxiliary camera. We fit the following Gaussian to the camera signal of the during images:

$$z(x,y) = z_0 + d\exp\left(2\frac{|x-x_0|^2+|y-y_0|^2}{w_0^2}\right) \tag{1}$$

Here, x and y are the spatial coordinates. d is the fitted maximum pixel count subtracted by the background. x_0 and y_0 are the fitted coordinates of the center of the peak intensity. w_0 is the fitted beamwaist. In Fig. 7, we show the beamwaist per illumination.

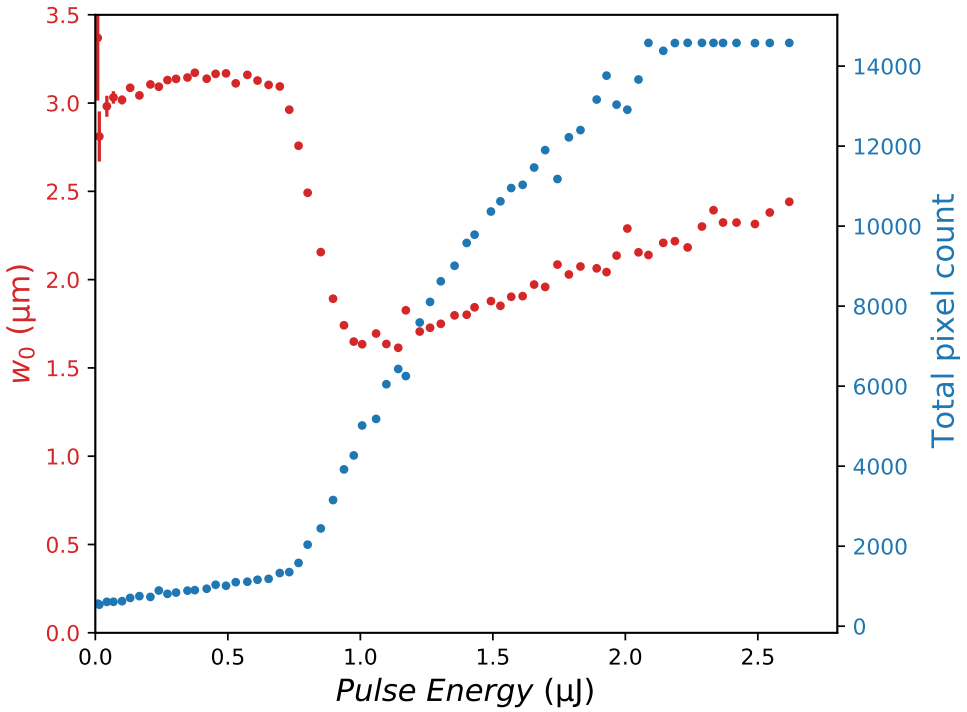

Figure 7: This figure shows the fitted beamwaist (red) and the maximum measured total pixel count (blue) as a function of pulse energy for the during images of PMMA on borosilicate glass at $\tau = 200$ fs.

We determined our beamwaist by selecting a regime where the total pixel count was still linear and where the signal to noise ratio of the self-reflectivity images was high. We assume the waist to be constant over the duration of an experiment. However, looking at fitted parameters in Fig. 7, this doesn't seem to be the case. This deviation can be understood by distinguishing 3 processes, coupled to 3 regimes of pulse energies. At very low pulse energies, there is little reflection, leading to a low signal to noise ratio on the camera. The low signal to noise ratio leads to poor fitting. At higher pulse energies, the signal to noise ratio becomes larger. In this pulse energy regime, we initially find that the total pixel count scales linearly with pulse energy. Starting from a pulse energy of 0.73 µJ, the slope of the total pixel count significantly increases. At the same pulse energy, the fitted beamwaist decreases. This can be explained by the fact that, at higher pulse energies, non-linear response of the electron density is starting to appear. This local increase in conduction band electron density leads to a local increase in self-reflectivity of the material. Because of this, Python will start to fit the beamwaist to the light reflected by the high density of conduction band electrons. Due to the Gaussian shape of the focus of the beam, the non-linear increase in conduction band electron density first appears where the center of the beam hits the sample, leading to a fitted beamwaist too small in size.
Considering these 3 regimes, we can conclude that the second regime represents the waist of the excitation pulses.
After inspection of the fitted beamwaists as a function of pulse energy for several τ, we conclude that the signal to noise ratio of regime 2 became better for longer pulse lengths. This is because the response remained linear for long pulse lengths at high pulse energies. For runs at $\tau = 20$ ps, we looked at the second regime and manually selected a beamwaist of 3.33 ± 0.05 µm.

4.1.3 A visual representation of OPR data of PMMA on glass

In Fig. 14, two overviews are shown, each representing a single run. Each overview consists of 64 individual depth maps. We use a dynamic divergent colormap where gray is the height of the background, blue represents values above the background level and darker colors represent heights lower than the background. The pulse

energy is lowest for the top left map and increases meanderingly. In this image, we mask pixels where the profilometer software couldn't determine a value and we mask unrealistic height fluctuations in nearest neighbour pixels (see Figure 14).

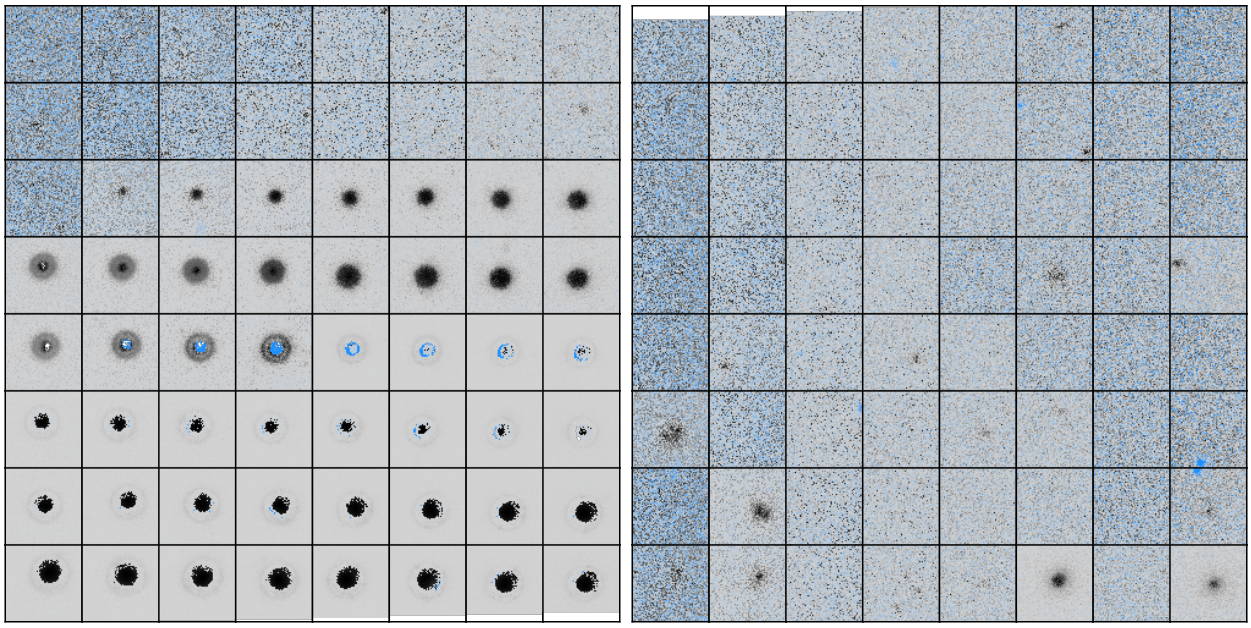

(a) (b)

Figure 8: An image from profilometry data at $\tau = 200$ fs (a) and at $\tau = 6$ ps (b). Per site the fluences increases linearly, starting at site 1 in the upper left meandering down to site 64 in the bottom right

One can see that a first crater appears at site 18 (1.65 J cm^{-2}). At site 29 (2.93 J cm^{-2}), we can see a crater within a crater starting to appear. In literature PMMA has a lower LIDT than glass (PMMA: 2.05 J cm^{-2} (26), glass: 2.6 J cm^{-2} (20)). Because of this, we expect that in the first crater only PMMA is removed and in the situation of a crater within a crater, both PMMA and glass are being ablated.
We assume the nature of the damage that we see in profilometry and aftermath images to be morphological. This assumption is based on the fact that the craters look well rounded. This doesn't mean that we exclude any chemical reactions. Based on the high energies being used, chemical reactions probably occur, but aren't apparent from these images. We observe a stochastic behavior in ablation in the profilometry overviews of runs with $\tau \geq 2$ ps. In these cases, at fixed τ, sometimes a site could show a crater whilst a site exposed to a higher fluence showed no damage.

4.1.4 Determination crater radius from profilometry data

From profilometry data, for every illumination site we defined the crater center as the minimum value. We fit the following 2D Gaussian to each individual height map:

$$z(x, y) = z_0 + d \exp\left(2\frac{|x - x_0|^2 + |y - y_0|^2}{r_0^2}\right) \tag{2}$$

d is the amplitude. x_0 and y_0 is the center coordinates of the crater. r is the fitted crater radius. Fig. 9 shows the cross section of several sites from profilometry data as an average over a range of 108 nm around y_0 at τ = 200 fs. We plot an average range instead of $y = y_0$ to suppress noise. Fig. 9 also shows the corresponding fitted Gaussians. The fitting procedure fails anywhere where no crater is present. In some other cases, the Gaussian failed to fit accurately to a crater even though the data seemed to show a crater.

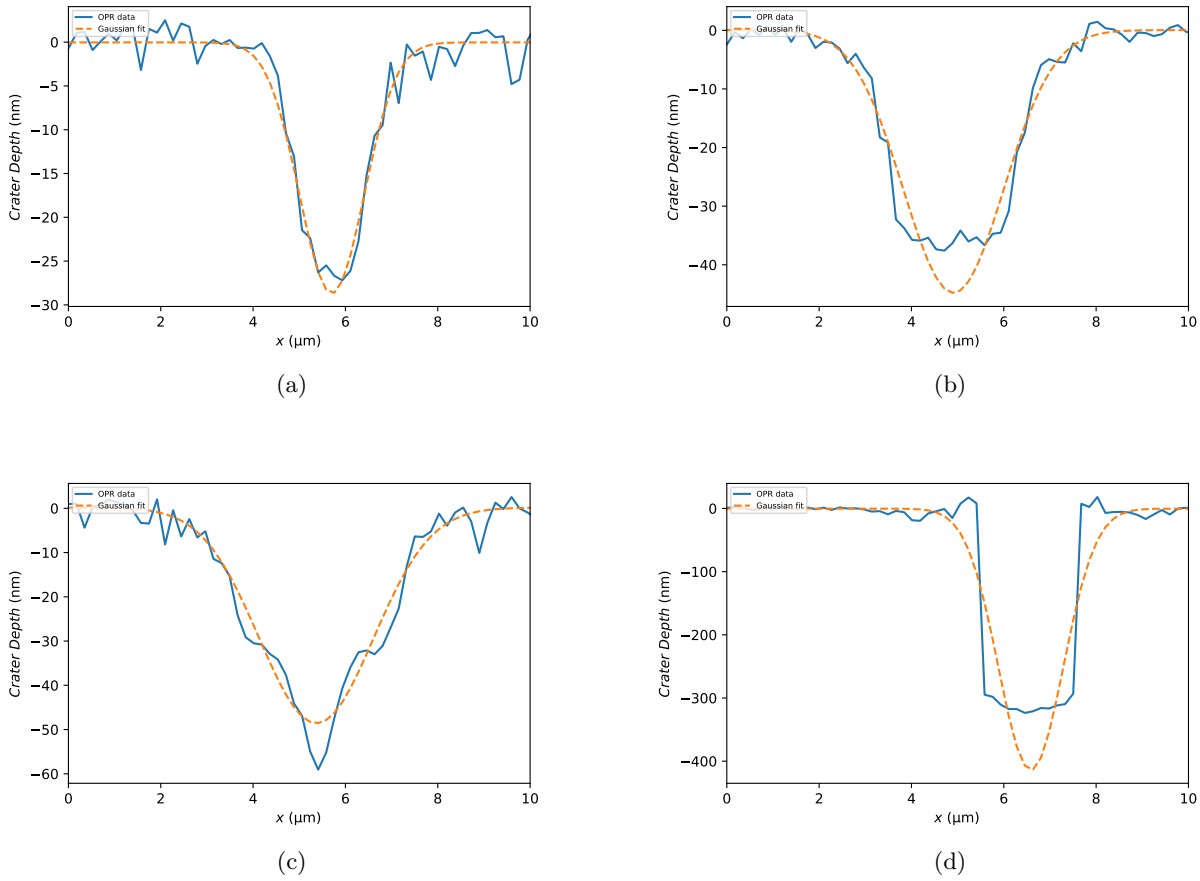

Figure 9: Cross sections and its corresponding fit of illumination sites at $\tau = 200$ fs for different fluences. The cross sections are averaged over a range of 108 nm around the center coordinate $y = y0$ to suppress noise. (a): $F = 1.74$ J, (b): $F = 2.43$ J cm^{-2}, (c): $F = 2.93$ J cm^{-2}, (d): $F = 5.41$ J cm^{-2}

In Fig. 9, 4 processes are visible. In Fig. 9a, a small crater is created with a parabolic shape. In Fig. 9b, the crater seems to flatten at the bottom. In Fig. 9c, a smaller crater starts to appear within the bottom of a crater. This process already became visible from a fluence of 2.57 J cm^{-2}, but we chose to show this cross section because the second crater is more visible. In Fig. 9d at 5.41 J cm^{-2}, the crater has become an order of magnitude deeper than the craters formed in Fig. 9a and Fig. 9b. Based on these observations and knowing that the PMMA layer is approximately 30 nm thick, we can assume that in Fig. 9a we ablate PMMA, but don't perforate it completely. In Fig. 9b we perforate the PMMA completely. The glass remains unharmed, which results in a flat bottom. In Fig. 9c, a crater in glass, within the PMMA crater, starts to appear. In Fig. 9d, PMMA and the borosilicate substrate are deeply perforated. Since the glass substrate is much thicker than the layer of PMMA, only the crater due to glass ablation is visible.

4.1.5 Crater depth of PMMA on glass

We define the crater depth as the average height of a surface with a radius of 0.27 µm around the center of the crater. Fig. 10 shows the crater depth as a function of pulse energy for a run at $\tau = 1$ ps and a run at $\tau = 3$ ps. It was clear that no crater was as large as an illumination site in profilometry data (10 µm × 10 µm) . Illumination sites for which the standard deviation of the crater depth was smaller than 10 nm were not used in analysis. We did this, because we assumed the profilimetry analysis program couldn't determine a clear height at these illumination sites. Also, Fig. 10 would become less clear if we would include crater depths with large standard deviations.

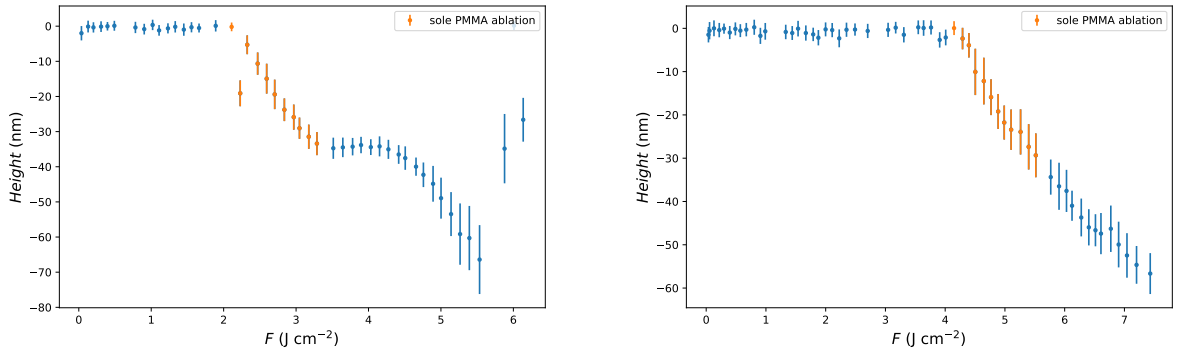

(a) (b)

Figure 10: The crater depth of the sample after illumination at different fluences for (a): $\tau = 1$ ps and (b): $\tau = 3$ ps. The regime of where we assume only PMMA is being ablated is colored orange

In Fig. 10a, one can see a first crater appearing at 2.22 J cm^{-2} and a second one around 4.28 J cm^{-2}. In Fig. 10a, we plot these data points and the data points in between in orange. Ablation followed by a flattening in crater depth was apparent for $\tau < 3$ ps. The flattening between fluences of 3.28 J cm^{-2} to 4.28 J cm^{-2} suggests the ablation of only one material, while the other one remains unharmed . The second material is than also ablated at 4.28 J cm^{-2}. The first ablated material was perforated to a depth of about 35 nm, which is very close to the reported thickness of the PMMA layer. The glass substrate is about 0,5 mm thick. This seems to confirm our hypothesis of PMMA being ablated before the borosilicate glass. At higher fluences, both the PMMA and the borosilicate glass are ablated.
From these figures, we wanted to determine the regime where only PMMA is ablated. At $\tau \geq 3$ ps, the flattening disappeared (see Figure 10b). This means that region between first ablation and flattening can't no longer be used as a criterion for the regime of where only PMMA is ablated. To still make use of the data of the longer pulselength runs, we assume craters which are shallower than the thickness of the PMMA layer, 35 nm, to be solely caused by PMMA ablation. In Fig. 10b, we plot these data points and the data points in between in orange. All craters deeper than 30 nm are not used in the analysis of the regime where only PMMA is ablated.
For some runs we can't determine the regime of where only PMMA is ablated. Some of these runs show no clear regimes of correlation between crater depth and fluence. Other runs which we can't use for analysis, are runs that don't have a sufficient number of illumination sites that show craters.

4.1.6 Laser-induced damage threshold of PMMA

Fig. 11 shows r^2, found in section 4.1.4, as a fucntion of the natural logarithm of the corresponding fluence for a run at $\tau = 200$ fs. We use two different fitting methods to find the LIDT of PMMA on borosilicate glass. One fitting method is a Liu fit (12). The other fit is based on a priori fixed beamwaist determined in section 4.1.2. Both methods fitted the following function to the regime of fluences where only PMMA is ablated. At $\tau = 200$ fs, this equation was also fitted to the regime of where glass started to be ablated.

$$r^2(x) = b_1(\log(x) - b_0) \tag{3}$$

For the Liu fit, x is the pulse energy E and $b_0 = \log(\text{LIDT} \cdot \pi w_0^2)$. For the fit using a fixed beamwaist, x is the fluence F and b_0 is $\log(\text{LIDT})$. The second fit was also used for the glass ablation at $\tau = 200$ fs. Not all fitted radii led to accurate results. Usually this is due to absence of a crater at the illumination site. Poor fitting due to absence of a crater is not a problem since only the regime where only PMMA is removed is relevant.

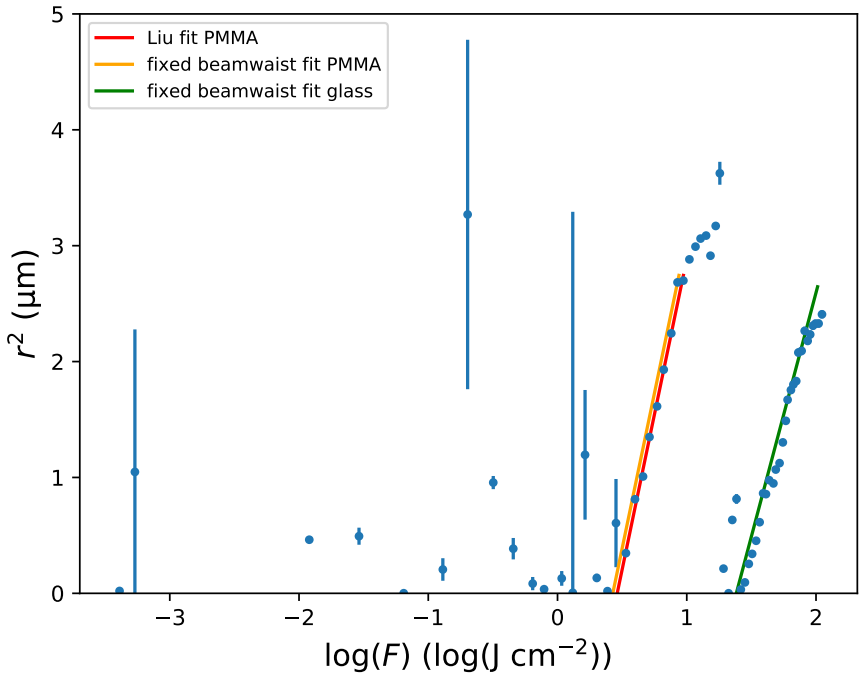

Figure 11: The square of the fitted crater radius r^2 as a function of $\log(F)$ at $\tau = 200$ fs. For PMMA, the lines for the Liu fit (orange) and for the fixed beamwaist fit (green) are also plotted. A fixed beamwaist fit for glass ablation is plotted as well.

In Fig. 11, we can see two linear trends. Both correspond two forming of a crater. We assign the first trend to a crater in the PMMA layer. We assign the second trend to the crater within the borosilicate glass and PMMA layer. The second linear trend was only visible for runs at $\tau = 200$ fs.
Fig. 11 shows the Liu fit to the first trend in red. In the Liu analysis, we determined the fluence, knowing the beamwaist $w_0 = \sqrt{2b_1}$. Assuming the LIDT is the fluence where r^2 becomes 0, $\frac{e^{b_0}}{\pi w_0^2}$ is the LIDT of PMMA on borosilicate glass.
We decided to do analysis with the fixed waist determined in 4.1.2 as well. This is the fit using a fixed beamwaist. Fig. 11 shows this fit for the crater in PMMA in orange and for the crater in both borosilicate glass and PMMA in green. For this fit, we determined the LIDT of PMMA for several τ and borosilicate glass at $\tau = 200$ fs as e^{b_0}.
For each pulse length 4 runs were measured. However, as stated in 4.1.5, we were not able to fit (3) to all runs. We combined per pulse length, the runs that yielded a LIDT to one value (see Figure 12).

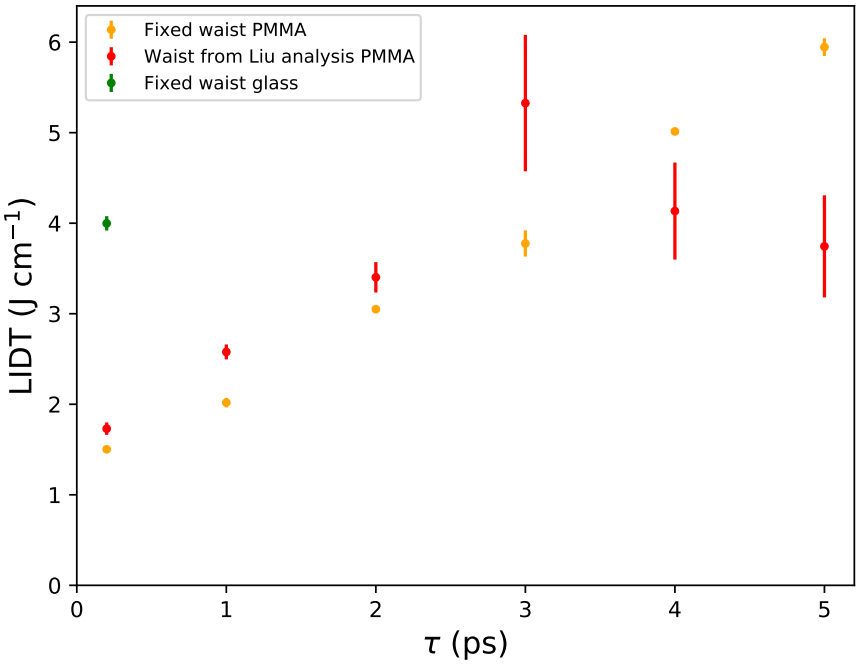

Figure 12: The LIDTs for PMMA on glass as function of different pulse lengths determined with a Liu analysis and a fit using a fixed beamwaist

Usually the LIDT increases with pulse length (7). In Fig. 12, this seems to be the case for the LIDTs determined with the fixed beamwaist (blue). For the Liu fit (orange), the LIDT at $\tau = 5$ ps shows no positive correlation when comparing to the LIDT of $\tau = 3$ ps. Looking at longer pulse lengths for LIDTs determined with the Liu fit, we see a decrease in precision, which leads us to assumption of the Liu fit becoming less reliable for longer pulse lengths in this experiment.

Both LIDts, are averages of 4 runs over 1 pulse length. The uncertainty is determined by the difference in these 4 values per pulse length.

4.2 Ablation and analysis of glass for different pulse durations

As reference measurement, we take a look at the depth profile after illumination of bare borosilicate glass. In this subsection we determine two LIDT for borosilicate glass. One LIDT is determined by manually selecting a site of first damage. The second LIDT is determined by looking at a decrease in slope of the fitted beamwaist as a function of fluence.

4.2.1 Ablation of glass

We repeated the experiment from section 4.1.1 on the backside of the same sample. Beside low-intensity illumination on front for imaging, we also illuminated the sample through transmission with the low-energy green LED.

4.2.2 Determination of the fluence

Between this experiment and the experiment of illumination of PMMA on borosilicate glass, we removed parts of the setup and moved, in our perception, them back into the the same spot. This leads us to assume that the beamwaist stayed constant. Fig. 13 shows both the fitted beamwaist (red) to self-reflectivity of the

sample captured with during images and the corresponding total pixel count (blue) as a function of pulse energy at $\tau = 20$ ps.

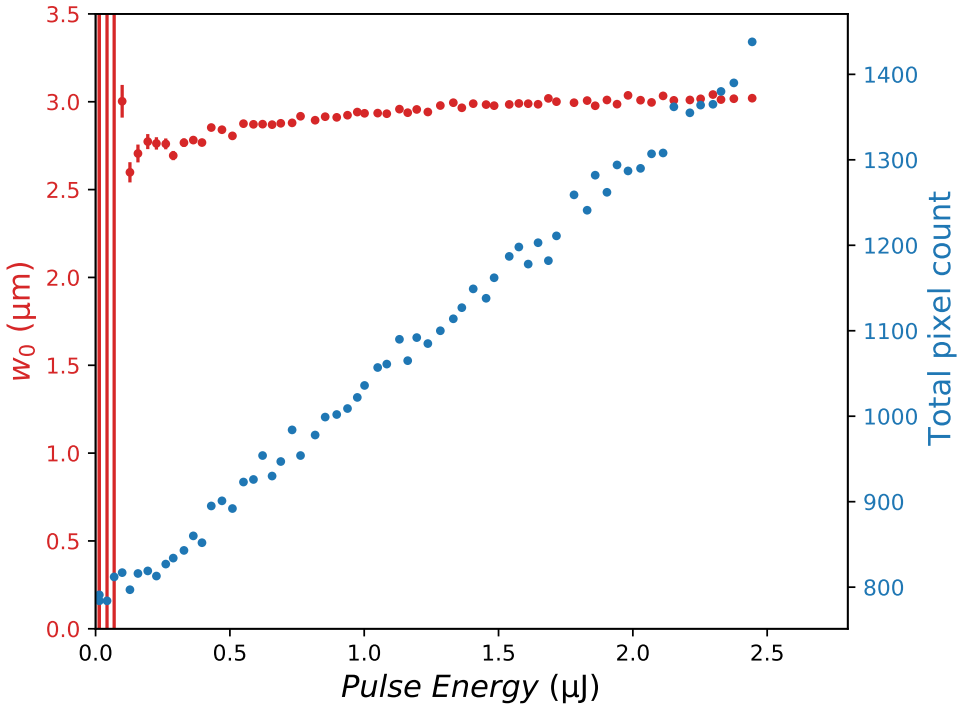

Figure 13: This figure shows the fitted beamwaist (red) and the maximum measured total pixel count (blue) as a function of pulse energy for the during images of bare borosilicate glass at $\tau = 20$ ps.

Fig. 13 shows no non-linear self-reflection of light at higher fluences. From this figure, and other figures at $\tau = 20$ ps, we estimate the beamwaist to be 3.03 ± 0.02 µm.
This is significantly smaller beamwaist than the beamwaist of 3.33 ± 0.05 µm we determined for the experiment in section 4.2. The only reason we can think of, is that this is due to a change in the experimental setup. To test this hypothesis, the experiment of section 4.2 and the experiment of this section should be conducted without making any alterations to the setup in between.

4.2.3 Determination of the LIDT of borosilicate glass from OPR images

Fig. 14a ($\tau = 200$ fs) and Fig. 14c ($\tau = 10$ ps) show two overviews of profilometry data of individual runs on borosilicate glass. These images are constructed in the same way as in Fig. 14. Fig. 14b and Fig. 14d are respectively the corresponding aftermath images for these profilometry images.

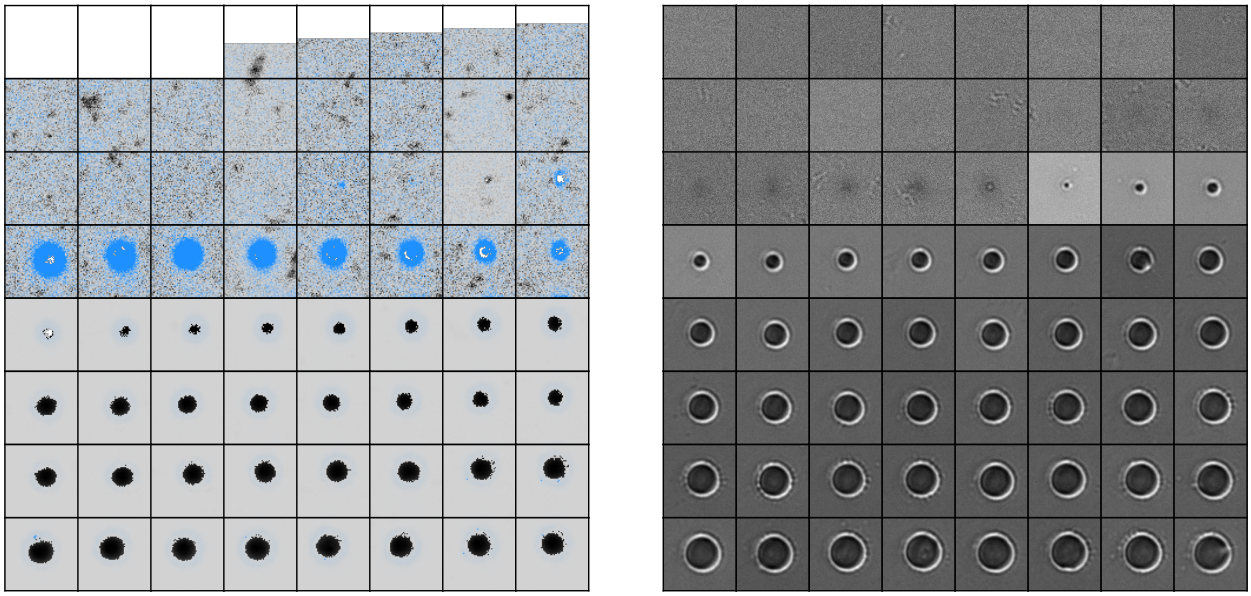

(a) (b)

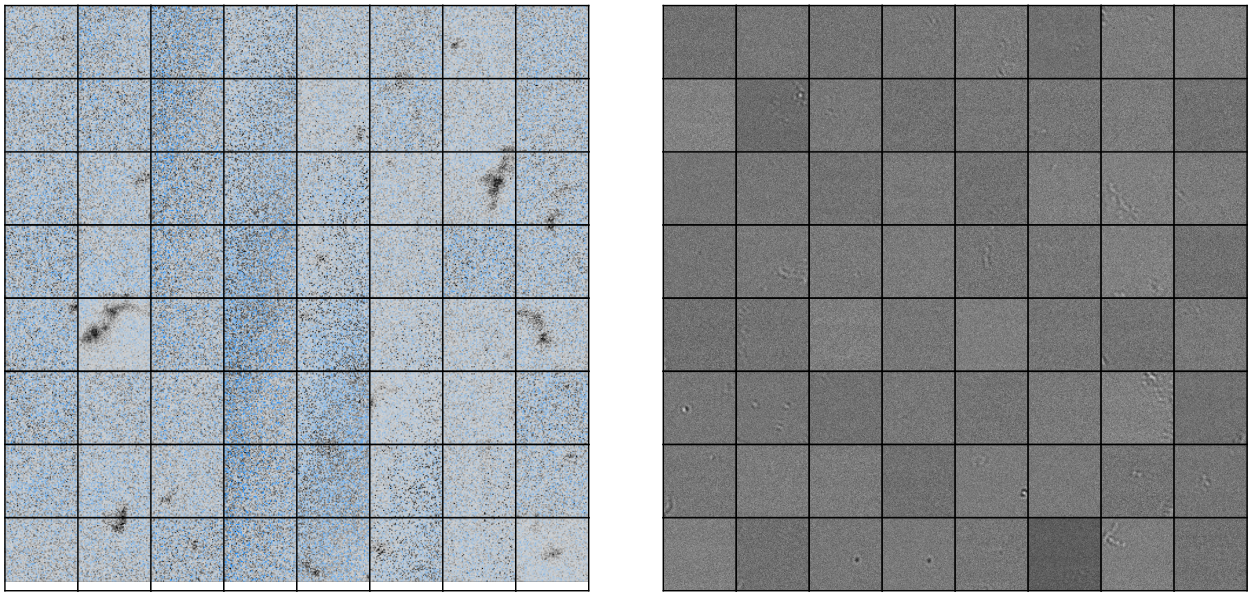

(c) (d)

Figure 14: Depth-map image constructed from profilimetry data for a run at $\tau = 200$ fs (a) and $\tau = 10$ ps (c) and their respectively their corresponding aftermath images for the corresponding runs (b) and (d). Per site, the fluence increases linearly, starting from site 1 in the upper left meandering down to site 64 in the bottom right

As in section 4.1.4, we fitted a Gaussian to the depth profile of the illumination sites. However, when plotting r^2 to $\log(F)$, there was no correlation to make a linear fit to for $\tau \geq 1$ ps. For this reason, we decide to determine the LIDT by averaging the fluence of the site of first damage and the site before. We determine the site of first damage by both looking at profilometry generated depth-map images and after-illumination

images. We take the half of the difference in fluence between the two sites to be standard deviation of the LIDT of borosilicate glass $\sigma^*_{LIDT,glass}$ for a single run.

There are a few complications in finding the LIDT this way. The first is that it is not always clear where damage was done to the substrate by the laser. In a lot of cases, it is hard to see at lower fluences, if a spot is an imperfection in the glass or that it is morphological change insinuated by illumination. Another complication, is that it is possible that there was a stochastic behavior in ablation. Fig. 14d shows an example of such a case when we look at site 59 (7.83 J cm^{-2}) and 60 (8.00 J cm^{-2}). In Figure 14c we don't see clear craters at these sites. This is likely because something went wrong determination of the sites in profilometer software for higher runs, which means Fig. 14c doesn't correctly show the sites of illumination.

We define the first site of ablation as the first site after which all sites show damage in the form of morphological change. When determining damage, we looked at all runs for $\tau \leq 5$ ps. Fig. 19 shows that at 5 ps, the ablation of PMMA does not show significant stochastic behaviour. We assume that damage won't be stochastic for $\tau \leq 5$ ps in illumination of borosilicate glass [1].

For the corresponding runs in the aftermath images (Fig. 14a and Fig. 14b), the first site of damage seems to differ. In the profilometry image Fig. 14a, we see that at site 21 ($F = 2.31$ J cm^{-2}), the height profile becomes positive. This can be labeled as damage according to our definition: change in morphology of the material.

In the aftermath image in Fig. 14b, we see a dark stain appearing at site 15 ($F = 1.64$ J cm^{-2}). This stain turns into a crater at site 21 ($F = 2.31$ J cm^{-2}). Considering our definition of damage, we should take the profilometry image as a leading image for damage, since it portrays change in morphology. Because of this, we consider the crater in aftermath image to be the first site of damage as well.

Fig. 8a shows the profilometry image for PMMA at $\tau = 200$ fs. First damage in this image is at a fluence of 1.65 J cm^{-2}. First damage for an illumination of $\tau = 200$ fs for borosilicate glass is 2.30 J cm^{-2}. This confirms our hypothesis of borosilicate glass having a higher LIDT than PMMA on borosilicate glass.

For each pulse length there are 4 runs. At a fixed site and pulse length, the fluence for one run might be a bit higher than for another run. Because of this, it is possible that for a fixed site and pulse length, for one run damage is visible while another run shows no damage. If one run shows damage at a higher site we discard this damage, because we're interested in the lowest value for LID. For the runs we don't discard, we take the average value to be the LIDT. We take the standard deviation of the LIDT of borosilicate glass $\sigma_{LIDT,glass}$ to be the avarage of $\sigma^*_{LIDT,glass}$ of the 4 runs at this pulse length.

Fig. 15 shows the LIDTs of borosilicate glass as a function of pulse length together with the LIDTs for PMMA on borosilicate glass we determined in section 4.1.6.

[1] In section 4.6 we find that, for illuminations $\tau \leq 5$ ps of PMMA on borosilicate glass, ablation does not show significant stochastic behaviour. Since we expect there to be less defects in borosilicate glass than in PMMA, we assume that there is no stochastic behavior in ablation of borosilicate glass for illuminations with $\tau \leq 5$ ps.

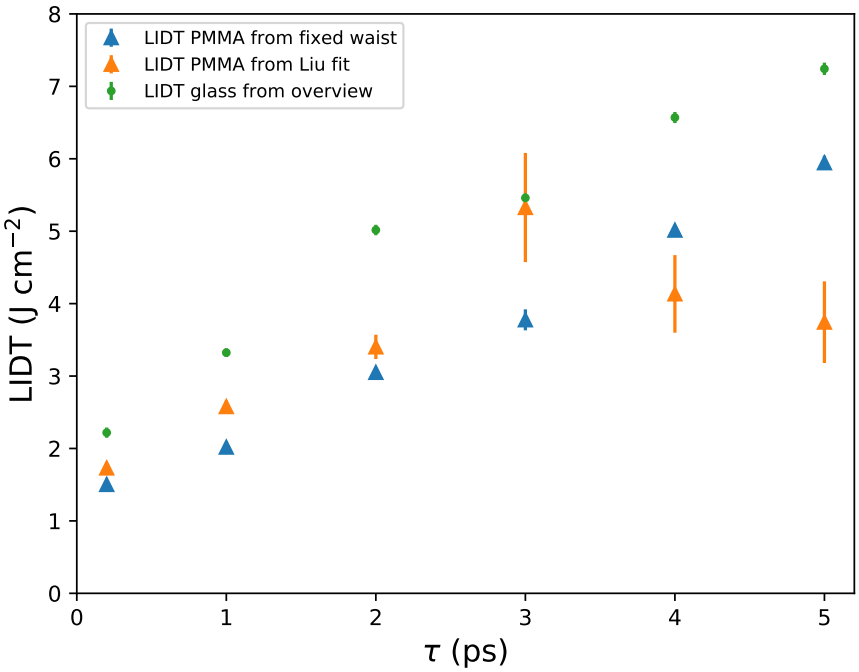

Figure 15: The LIDTs of borosilicate glass and PMMA as a function of different pulselengths. We determined the LIDTs of borosilicate glass by manually selecting the sites of first damage in profilometry and aftermath images. We determined the LIDTs of PMMA in section 4.1.6 by fitting using a fixed beamwaist and a Liu fit.

As we expect we can see an increase in LIDT with pulse length. For fixed pulse lengths, the LIDT of borosilicate glass is higher than the one of PMMA on borosilicate glass (see Figure 12). This is in agreement with our hypothesis.

4.3 Determination of the LIDT of borosilicate glass from reflections of the laser-beam

Fig. 16 shows the fitted beamwaist for both PMMA on borosilicate glass and borosilicate glass as a function of fluence at. Fig. 16 also shows the LIDT of borosilicate glass (from overview images) and the LIDT of PMMA (from a fixed beamwaist fit).

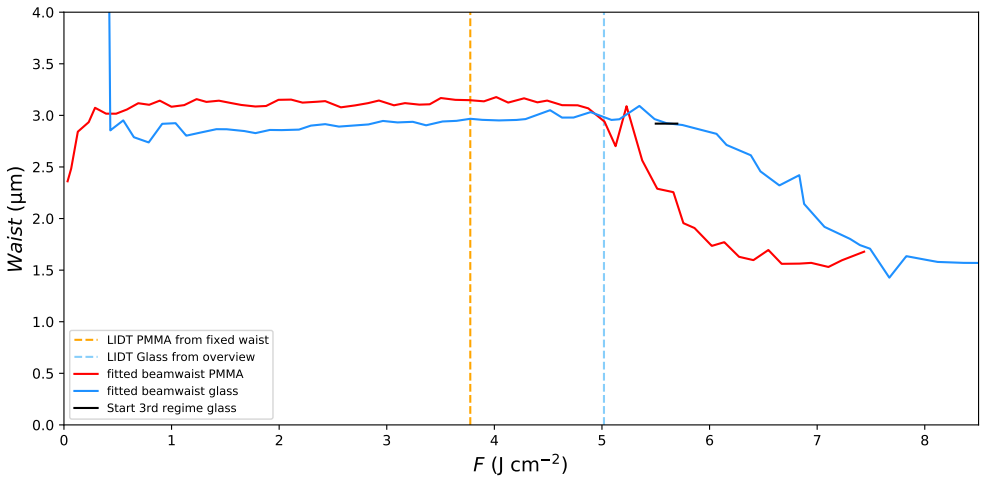

Figure 16: The fitted beamwaist to both reflections of PMMA on glass and bare glass at $\tau = 3$ ps. The figure also shows the determined LIDT of PMMA for a fixed beam waist and the LIDT of glass determined from overview along the y-axis. A black line is plotted to show the manually determined start of the regime of locally enhanced self-reflectivity.

In section 4.1.2 we described three regimes for the fitted beamwaists as a function of fluence. For most cases, the LIDT of glass, determined from overview images, seems to be at the same fluence as the start of the regime of locally enhanced self-reflectivity. Our explanation is that these quantities are both caused by a non-linear increase in the conduction band electron density. Based on this explanation, we can assume the LIDT of borosilicate glass is equal to fluence of the start of the regime of locally enhanced self-reflectivity. Fig. 17 shows these new LIDTs together with LIDTs of borosilicate glass determined from overview images and the LIDT of PMMA determined from a fit using a fixed beamwaist.

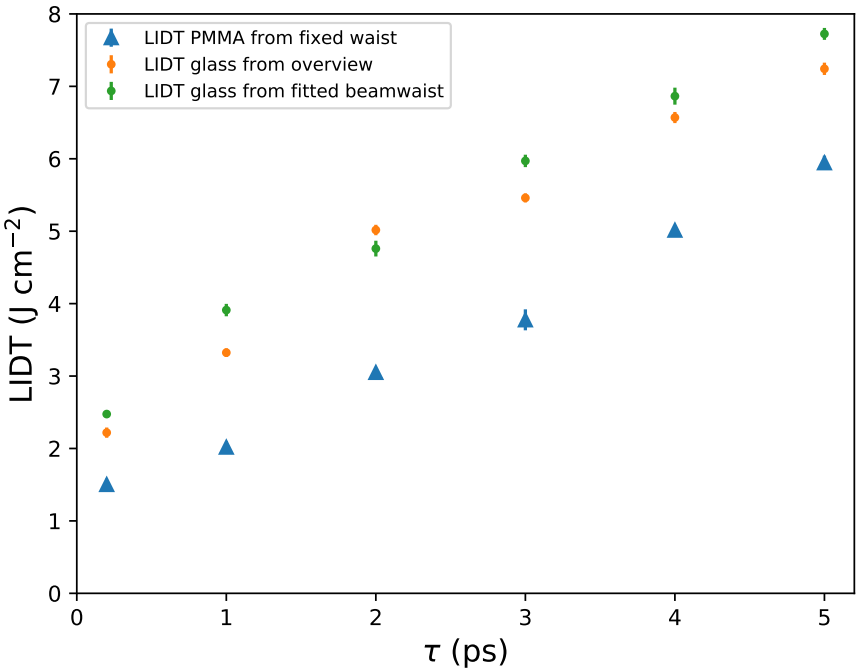

Figure 17: The LIDTs for borosilicate glass as a function of different pulse lengths both determined by looking at first damage in profilometry and transmission images and by looking at reduction in fitted beamwaist

We determined the newly found LIDTs by looking at the change in fitted beamwaist. We assume both damage and reduction in size of fitted beamwaist are caused by a strong non-linear increase in conduction band electron density. This means we indirectly determine this LIDT of borosilicate glass.

4.4 Differences in damage to PMMA on borosilicate glass and bare borosilicate glass

As stated above, we attribute the damage to bare borosilicate glass to a non-linear increase conduction band electron density. Fig. 16 shows that the LIDT of PMMA on glass is at a lower fluence than the start of the regime of locally enhanced self-reflectivity. Recalling section 2.1, borosilicate glass has a melting point of $>$ 800 °C. The melting point of PMMA is dependent on degree of polymerization but is considerably lower than 800 °C. From 220 °C PMMA can undergo an exothermic decomposition reaction in presence of water and oxygen. We don't know the timescale on which this decomposition reaction would be initiated. If the layer of PMMA is not at a temperature which is sufficient to initiate this reaction for long enough, we assume that the distinguishable damage seen in profilometry data is of non-chemical origin. If the decomposition reaction is on the timescale of increase in temperature of PMMA, the chemical reaction could have an increasing effect on the morphological change. As stated in 2.1, the products of the decomposition reaction of PMMA have a lower melting point. This is because of their lower degree of polymerization (DP) than the original PMMA chain.

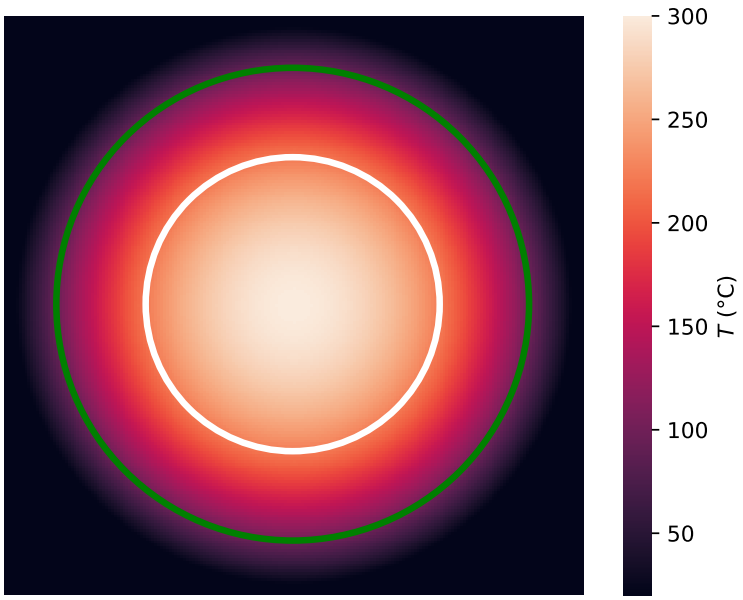

Figure 18: An illustration of a heated illumination site. The center of the illumination site is 300 °C and linearly cools down to 20 °C as a function of distance from the center. The white line marks 220 °C, the lowest decomposition temperature for PMMA. The green line marks 98 °C, the melting temperature for PMMA with DP = 28 .

In Fig. 18, the morphological change for PMMA chains with a DP that has a melting point of > 220 °C would only be visible inside the white ring if one would only assign the morphological change to melting. However, if these PMMA chains would undergo a decomposition reaction, the melting point of the products would presumably be lower. This would extend the area in which morphological change is visible. In Fig. 18 the green ring represents 98 °C, the melting point of PMMA with DP = 28.
Fig. 18 represent an illumination site with a temperature of 300 °C at the center. The temperature decreases linearly from the center to 20 °C. If decomposition happens at some time interval to PMMA after illumination, it is unclear how the material has cooled down during this time interval. This means, if morphological change is dependent on chemical decomposition, it is unclear what the role of this decomposition is in the total morphological change of the site. It also means that in Fig. 18, the ratio of the green and the white circle should not be considered as quantitatively accurate.
In order to qualitatively understand LID to PMMA on borosilicate glass, one should further investigate timescales of local cooling and decomposition reactions of PMMA on borosilicate glass after illumination. One could also investigate the local DP of PMMA before and after illumination.

4.5 Disappearance of the flattening between PMMA and borosilicate glass ablation at longer pulse lengths

Fig. 10a ($\tau = 200$ fs) shows a regime where PMMA is completely perforated, while glass remains unharmed. This results in flattening of the curve. Fig. 10b ($\tau = 3$ ps) no longer shows this flattening. Fig. 15 shows that the LIDT of glass is 5.46 ± 0.06 J cm^{-2} at $\tau = 3$ ps. Fig. 10b shows that the crater has a depth of 29 ± 5 nm at the same pulse length and roughly the same fluence ($F = 5.52$ J cm^{-2}). If we consider crater depths as a function of fluence at $\tau \leq 3$ ps, at about 35 nm the the bottom of the PMMA layer is reached. This is approximately the height of the crater. For higher pulse lengths, at the LIDT of bare borosilicate

glass, the crater is even less deep. An explanation for disappearance of the flattening during ablation could be that the fluence is high enough to perforate the glass as soon as the PMMA is completely perforated for $\tau \geq 3$ ps. For $\tau < 3$ ps, the fluence upon complete perforation of the PMMA layer is smaller than the LIDT of bare borosilicate glass, causing flattening. One should consider that the LIDT of bare borosilicate glass will be lower than the LIDT of the borosilicate glass substrate under PMMA, since the PMMA on top will absorb (part of the) light. Because of this, we expect the disappearance of flattening to become apparent if the fluence upon complete perforation of the PMMA layer is significantly higher than the LIDT of bare borosilicate glass at the same pulse length.

4.6 Stochastic LID of PMMA on borosilicate glass

In section 4.1.3 we observe a stochastic behaviour in ablation process for several runs (see Fig. 8b). To better understand this process, we determine the damage probability of PMMA in regimes of pulse lengths and fluences. We selected these regimes to be the same regimes as the ones that showed stochastic behaviour in the experiment of section 4.1. We again did an experiment illuminating several sites of PMMA on borosilicate glass. The pulse lengths that were chosen were 1 ps, 3 ps, 5 ps, 7 ps, 9 ps, 11 ps, 16 ps and 20 ps. We linearly increased the fluences from approximately 4.5 J cm^{-2} to 6.4 J cm^{-2}. For every pulse length-fluence combination we illuminated 32 sites.
To analyze the data, a script in python showed one aftermath site at the time in random order. By eye, we determined if a crater was formed per site. We double checked this analysis by comparing the aftermath images containing one entire run with a corresponding binary map (1 = crater, 0 = no crater) of the data from the python script. When comparing these sites, the pulse length and the fluence were not shown. Fig. 19 shows the damage probability as a function of fluence for the different pulse lengths.

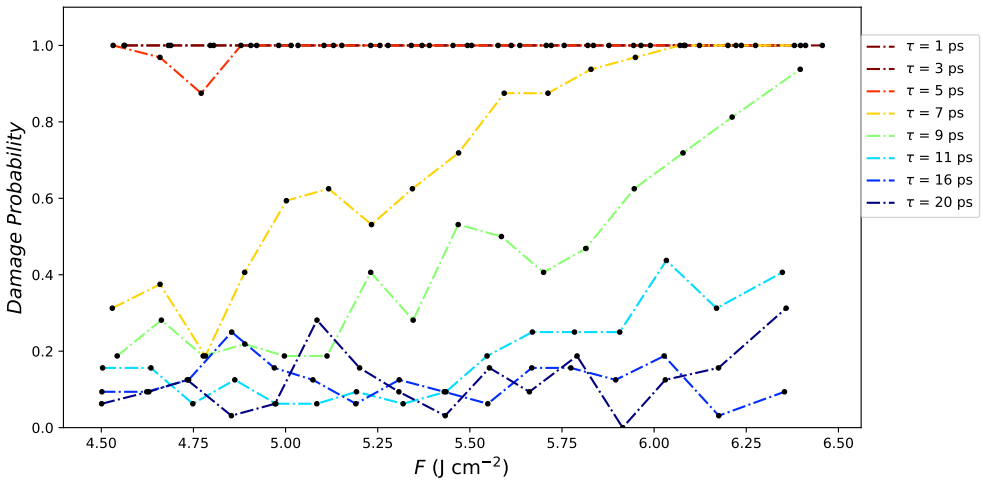

Figure 19: The damage probability for PMMA as a function of fluence for different pulse lengths

Fig. 19 shows an increasing damage probability as function of fluence for $\tau = 7$ ps, 9 ps, 11 ps. $\tau \geq 16$ ps the damage probability stays close to 0. For $\tau \leq 3$ the damage probability is close to 1 for all fluences.
An explanation for the stochastic ablation could be the excitation/ionization of valence electrons via trap states due to defects at some site sites of illumination. Another explanation could be the presence of inclusions (18). Photoluminescence microscopy analysis suggested that the PMMA was very homogeneous. We don't expect inclusions to be visible in photoluminescence microscopy. It is also possible that defects didn't show, although they were present.

5 Conclusion

In this work, we found, through different methods, light induced damage thresholds (LIDTs) for both PMMA and borosilicate glass. In almost all cases the LIDT increased with the pulse length (τ). This trend is what we expected, based on literature. Only the LIDT of PMMA, found by the Liu fit, showed deviation from this trend at higher pulse lengths. We attribute this deviation to a non-physical fitting artifact.
All LIDTs for bare borosilicate glass were higher than the LIDTs for PMMA on borosilicate glass at corresponding pulse lengths. This was expected as well, based on literature.
We found that the LIDT of borosilicate glass corresponds to the fluence at which the self-reflectivity of the excitation pulse at the surface is locally enhanced. We assign both of these phenomena to a non-linear increase in conduction band electron density. This means we can assume that the LIDT of borosilicate glass is equal to the fluence of where the self-reflectivity becomes locally enhanced. We assign the differences in the observed behavior between glass and PMMA on glass to PMMA having a significantly lower melting point. A hypothesis which could also explain why PMMA breaks down before the non-linear increase in conduction band electron density, could be chemical decomposition of PMMA. This decomposition would result in reaction products with a presumably lower melting point than the original PMMA chain. To investigate this hypothesis, the timescale of melting and chemical decomposition for PMMA can be further looked into. One could also investigate the local degree of polymerization of PMMA before and after exposure of light.
One remarkable observation that we made while studying damage in PMMA on glass is that for short pulse lengths, we determined a flattening in crater depth as a function of fluence. We assign this flattening to borosilicate glass having a higher LIDT than PMMA on glass. For short pulse lengths, the fluence at which PMMA is completely perforated is not high enough to ablate the glass. This results in flattening. For longer pulse lengths, this flattening disappeared. We assign this to PMMA being perforated less deeply for a fixed fluence with increasing pulse lengths. At longer pulse lengths, the fluence at which the PMMA is completely perforated, is high enough to ablate the glass substrate. This fluence should be higher than the LIDT found for bare borosilicate glass, since part of the pulse energy is already absorbed by the layer of PMMA before reaching the borosilicate glass substrate.
For both PMMA on glass and glass, at certain fluence-pulse length regimes, ablation became a stochastic process. For PMMA on borosilicate glass, we examined these regimes by determining damage probability as a function of fluence for different τ. In this damage probability analysis, we found a regime of pulse lengths where the damage probability clearly decreased with the pulse length. For long pulse lengths the damage probability stayed low for all fluences. For short pulse lengths, the damage probability stayed close to 1 for all fluences. The mechanism behind this stochastic ablation is yet to be determined. We performed photoluminescence on the sample, which showed it to be homogeneous. This does not mean that the presence of defects or inclusions is excluded. To understand this stochastic behavior in ablation, further chemical analysis can be done.

References

[1] Al-Bataineh, Q. M., Ahmad, A. A., Alsaad, A., and Telfah, A. D. (2021). Optical characterizations of pmma/metal oxide nanoparticles thin films: bandgap engineering using a novel derived model. *Heliyon*, 7(1):e05952.

[2] Ali, U., Karim, K. J. B. A., and Buang, N. A. (2015). A review of the properties and applications of poly (methyl methacrylate)(pmma). *Polymer Reviews*, 55(4):678–705.

[ASML] ASML. Asml - powering the next phase of semiconductor manufacturing.

[4] Baum, A., Scully, P. J., Basanta, M., Thomas, C. P., Fielden, P. R., Goddard, N. J., Perrie, W., and Chalker, P. R. (2007). Photochemistry of refractive index structures in poly (methyl methacrylate) by femtosecond laser irradiation. *Optics letters*, 32(2):190–192.

[5] Du, J., Wu, J., Zhao, L., and Song, L. (2013). Color centers of a borosilicate glass induced by 10 mev proton, 1.85 mev electron and 60co-γ ray. *Radiation Physics and Chemistry*, 86:59–63.

[6] Eremyashev, V., Zherebtsov, D., Osipova, L., and Danilina, E. (2016). Thermal study of melting, transition and crystallization of rubidium and cesium borosilicate glasses. *Ceramics International*, 42(16):18368–18372.

[7] Gedvilas, M. and Račiukaitis, G. (2005). Investigation of uv picosecond laser ablation of polymers. In *Workshop on Laser Applications in Europe*, volume 6157, pages 70–79. SPIE.

[8] He, G. S., Tan, L.-S., Zheng, Q., and Prasad, P. N. (2008). Multiphoton absorbing materials: molecular designs, characterizations, and applications. *Chemical reviews*, 108(4):1245–1330.

[9] Héberger, K. and Lopata, A. (1998). Assessment of nucleophilicity and electrophilicity of radicals, and of polar and enthalpy effects on radical addition reactions1. *The Journal of Organic Chemistry*, 63(24):8646–8653.

[10] Jia, T.-q., Chen, H., and Zhang, Y.-m. (2000). Photon absorption of conduction-band electrons and their effects on laser-induced damage to optical materials. *Physical Review B*, 61(24):16522.

[11] Lenzner, M., Krüger, J., Sartania, S., Cheng, Z., Spielmann, C., Mourou, G., Kautek, W., and Krausz, F. (1998). Femtosecond optical breakdown in dielectrics. *Physical review letters*, 80(18):4076.

[12] Liu, J. (1982). Simple technique for measurements of pulsed gaussian-beam spot sizes. *Optics letters*, 7(5):196–198.

[13] Nieto, D., Arines, J., O'Connor, G. M., and Flores-Arias, M. T. (2015). Single-pulse laser ablation threshold of borosilicate, fused silica, sapphire, and soda-lime glass for pulse widths of 500 fs, 10 ps, 20 ns. *Applied optics*, 54(29):8596–8601.

[14] Popov, V. S. (2004). Tunnel and multiphoton ionization of atoms and ions in a strong laser field (keldysh theory). *Physics-Uspekhi*, 47(9):855.

[15] Rahman, F., Carbaugh, D. J., Wright, J. T., Rajan, P., Pandya, S. G., and Kaya, S. (2020). A review of polymethyl methacrylate (pmma) as a versatile lithographic resist–with emphasis on uv exposure. *Microelectronic Engineering*, 224:111238.

[16] Rethfeld, B., Sokolowski-Tinten, K., Von Der Linde, D., and Anisimov, S. (2004). Timescales in the response of materials to femtosecond laser excitation. *Applied Physics A*, 79(4):767–769.

[17] Ristau, D. (2014a). *Laser-induced damage in optical materials*, pages 127–140. CRC Press.

[18] Ristau, D. (2014b). *Laser-induced damage in optical materials*, page 22. CRC Press.

[19] Ristau, D. (2014c). *Laser-induced damage in optical materials*, pages 188–189. CRC Press.

[20] Smedskjaer, M. M., Mauro, J. C., Youngman, R. E., Hogue, C. L., Potuzak, M., and Yue, Y. (2011). Topological principles of borosilicate glass chemistry. *The Journal of Physical Chemistry B*, 115(44):12930–12946.

[21] Ute, K., Miyatake, N., and Hatada, K. (1995). Glass transition temperature and melting temperature of uniform isotactic and syndiotactic poly (methyl methacrylate) s from 13mer to 50mer. *Polymer*, 36(7):1415–1419.

[22] Vance, E., Begg, B., and Gregg, D. (2017). Immobilization of high-level radioactive waste and used nuclear fuel for safe disposal in geological repository systems. In *Geological Repository Systems for Safe Disposal of Spent Nuclear Fuels and Radioactive Waste*, pages 269–295. Elsevier.

[23] Vreugdenhil, M. (2020). Electron-induced carrier dynamics in semiconductors. Master's thesis.

[24] Yablonovitch, E. and Bloembergen, N. (1972). Avalanche ionization and the limiting diameter of filaments induced by light pulses in transparent media. *Physical Review Letters*, 29(14):907.

[25] Yousif, E., El-Hiti, G. A., Haddad, R., and Balakit, A. A. (2015). Photochemical stability and photostabilizing efficiency of poly (methyl methacrylate) based on 2-(6-methoxynaphthalen-2-yl) propanoate metal ion complexes. *Polymers*, 7(6):1005–1019.

[26] Žukauskas, A., Batavičiūtė, G., Ščiuka, M., Jukna, T., Melninkaitis, A., and Malinauskas, M. (2014). Characterization of photopolymers used in laser 3d micro/nanolithography by means of laser-induced damage threshold (lidt). *Optical Materials Express*, 4(8):1601–1616.

[27] Vreugdenhil, M., Van Oosten, D. (2022). A highly automated apparatus for ultra-fast laser ablation studies [Unpublished manuscript]. Nanophotonics, Utrecht University.